Social distancing in pedestrian dynamics and its effect on disease spreading

Sina Sajjadi [1,2,3,*] Alireza Hashemi [1,*] and Fakhteh Ghanbarnejad [1,4,†]

[1] *Department of Physics, Sharif University of Technology, P.O. Box 11165-9161, Tehran, Iran*

[2] *Complexity Science Hub Vienna, Vienna, Austria*

[3] *Central European University, Vienna, Austria*

[4] *Chair for Network Dynamics, Institute for Theoretical Physics and Center for Advancing Electronics Dresden (cfaed), Technical University of Dresden, 01062 Dresden, Germany*

(Received 6 November 2020; revised 6 April 2021; accepted 26 May 2021; published 26 July 2021)

Nonpharmaceutical measures such as social distancing can play an important role in controlling the spread of an epidemic. In this paper, we use a mathematical model combining human mobility and disease spreading. For the mobility dynamics, we design an agent-based model consisting of pedestrian dynamics with a novel type of force to resemble social distancing in crowded sites. For the spreading dynamics, we consider the compartmental susceptible-exposed-infective (*SEI*) dynamics plus an indirect transmission with the footprints of the infectious pedestrians being the contagion factor. We show that the increase in the intensity of social distancing has a significant effect on the exposure risk. By classifying the population into social distancing abiders and nonabiders, we conclude that the practice of social distancing, even by a minority of potentially infectious agents, results in a drastic change in the population exposure risk, but it reduces the effectiveness of the protocols when practiced by the rest of the population. Furthermore, we observe that for contagions for which the indirect transmission is more significant, the effectiveness of social distancing would be reduced. This study can help to provide a quantitative guideline for policy-making on exposure risk reduction.

DOI: 10.1103/PhysRevE.104.014313

I. INTRODUCTION

The ongoing COVID-19 pandemic has had severe consequences on nations worldwide. It has been considered to be one of the costliest disasters after WWII, and it has imposed many costs to local, regional, and global markets, including hundreds of billions to the global insurance industry, tourism, and other businesses. Facing these difficulties, governments have turned to nonpharmaceutical measures such as social distancing to limit the transmission of the disease and to hinder the growth of the spreading dynamics [1]. Motivated by this situation, we mathematically study the *effectiveness* of social distancing and how it can be implemented in order to reduce the risk of spreading.

Following the early work of Kermack and McKendrick [2] researches have implemented compartmental models, i.e., categorizing the population into collectively exhaustive compartments, meaning that every agent is a member of one and only one compartment, to describe and predict the epidemic dynamics. While the initial studies in this field were mostly focused on mean-field approximations [3], later on, a large body of work was concentrated on network studies with either analytical or computational approaches [4,5]. And then due to the greater access to agent level interaction data, the role of temporality of interactions got more attention in the studies [6–10].

Mobility of agents has been studied with different approaches, including pedestrian dynamics introduced in [11]. While this model has been widely implemented and studied, only recently was it used to model transmission processes. For example, Refs. [12] and [13] study the level of exposure of individuals to the infection, while Refs. [14–16] develop population level equations, and Refs. [17–19] introduce agent-based models to study the spreading in pedestrian dynamics.

In this work, we define a novel type of social distancing (keeping distance from other agents to avoid infection) based on the pedestrian dynamics. We also study the indirect transmission by taking into account the role of the environment as a vehicle of spreading [20]. We will investigate the system for different scenarios and a range of parameters. We show where social distancing is *executable* and how it can be *effective* for decreasing the *exposure risk*, however in some parameter regimes, the increase in indirect transmission may cancel the *effectiveness* of social distancing. As we will discuss, our results can help in devising a quantitative guideline for policy-making on reducing the exposure risk for many contagions, including SARS-CoV-2.

II. MODEL

A. Mobility of the agents

We simulate the walking patterns of people in a closed environment. For this purpose, we implement a formulation of the pedestrian dynamics introduced in [11], including a novel type of social distancing force. Agents aim to reach randomly chosen destinations while trying to keep distance from other agents and physical barriers (e.g., walls). Although the actual Newtonian forces do not have a direct impact on the dynamics, as humans rarely have physical contact with each

*These authors contributed equally to this work.

†fakhteh.ghanbarnejad@gmail.com

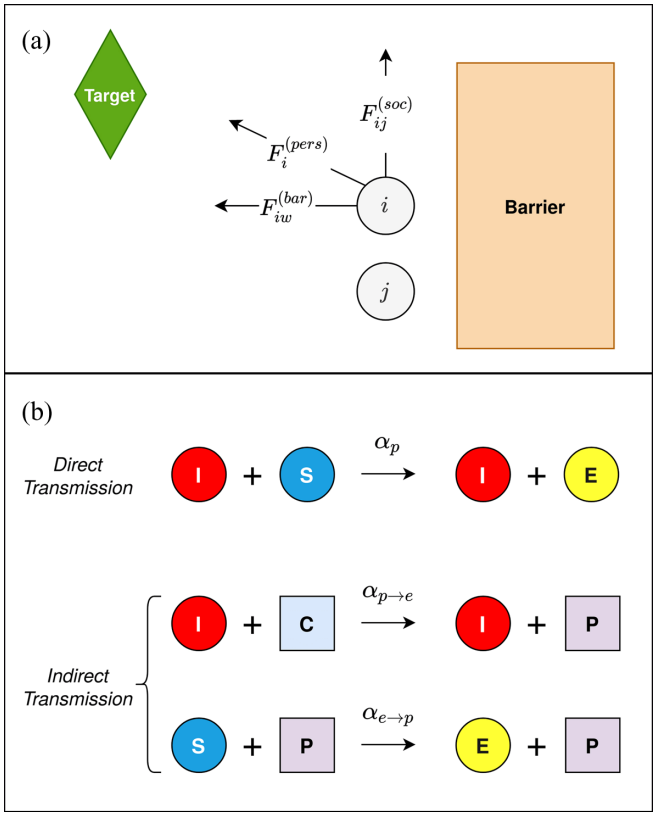

FIG. 1. A schematic illustration of the model. (a) The mobility model: three types of forces exerted on agent i, described in Sec. II A. Each agent chooses a random target and moves toward it ($\mathbf{F}_i^{(\text{pers})}$) while keeping distance from other agents ($\mathbf{F}_{ij}^{(\text{soc})}$) and physical barriers ($\mathbf{F}_{iw}^{(\text{bar})}$) [see Eq. (4)]. (b) The spreading model: the two types of contagion spreading described in Sec. II B as direct transmission (due to person to person contact of the agents) and indirect transmission (due to the polluted environment). Circles represent agents, while S, E, I denote the compartments to which they belong. Squares represent tiles of the environment, with C and P, respectively, representing clean and polluted tiles. The figure in Appendix A 3 depicts snapshots of the simulation for different values of σ. An mp4 animation demonstrating a sample realization of the dynamics can be found in Appendix A 3.

other/barriers while moving, taking into account the social pseudoforces governing a person's movement patterns enables us to study this issue in a physical framework. This method has achieved realistic results confirmed with experimental data [21].

As depicted in Fig. 1(a), in this dynamics each agent's movement is governed by three forces:

(i) *Personal force* $\mathbf{F}_i^{(pers)}$: Each agent i has a tendency to move with a velocity vector $\mathbf{v}_i^0 = v_i^0 \hat{\mathbf{v}}_i^0$, with v_i^0 being the preferred walking speed and $\hat{\mathbf{v}}_i^0$ the normal vector toward its chosen destination. This tendency is expressed in Eq. (1) as follows:

$$\mathbf{F}_i^{(pers)} = m_i \frac{\mathbf{v_i}^0 - \mathbf{v}_i}{\tau}, \tag{1}$$

where $\mathbf{v}_i$ denotes the agent's current velocity, m_i is its mass, and τ refers to the reaction time. The preferred walking speed v_i^0 will be set to 1.3 in agreement with empirical studies [22] as well as previous simulations of pedestrian dynamics [11]. Reaction time τ has also been calibrated in [11] and will be set to 0.5 for our study.

(ii) *Social force* $\mathbf{F}_{ij}^{(soc)}$: Every agent i tries to keep distance from every other agent j. This tendency can be modeled by a decreasing force, a function of their relative distance r_{ij}, with the direction of the force being the normalized vector $\hat{\mathbf{r}}_{ij}$ pointing from agent j to i. In this research, we consider the exponential force as in Eq. (2), introducing σ_i as a measure for agent i's tendency to abide by social distancing. We also consider r_c as the cutoff distance for the simulation purposes, i.e., agents do not exert any force on other agents beyond $r_c = 3$,

$$\mathbf{F}_{ij}^{(\text{soc})} = \kappa \sigma_i e^{-\frac{r_{ij}}{\sigma_i}} \hat{\mathbf{r}}_{ij}. \tag{2}$$

In real-life situations, the values for σ_i and κ would be determined by the behavior of the agents in different environments. For example, people tend to walk closer together in a shopping mall and farther apart when taking an afternoon walk in a park. σ_i can be used to represent the idea of social distancing in a community of agents. With a higher value for σ_i, agent i would tend to stay farther apart from other agents. For simplicity, we consider κ to be a constant and set $\kappa = 7$. This conforms with the previous research on pedestrian dynamics [11].

(iii) *Barrier avoidance force* $\mathbf{F}_{iw}^{(bar)}$: Agents avoid barriers in the same manner that they avoid other agents as expressed in Eq. (3), with σ_w being the uniform tendency to keep distance from physical barriers, and κ_w as the force constant. In our study, the only barriers would be the walls surrounding the environment,

$$\mathbf{F}_{iw}^{(\text{bar})} = \kappa_w \sigma_w e^{-\frac{r_{iw}}{\sigma_w}} \hat{\mathbf{r}}_{iw}. \tag{3}$$

Although, as stated, these are not Newtonian forces, we can obtain the equation of motion for each agent i as expressed in Eq. (4),

$$m_i \frac{d\mathbf{v}_i}{dt} = \mathbf{F}_i^{(\text{pers})} + \mathbf{F}_{ij}^{(\text{soc})} + \mathbf{F}_{iw}^{(\text{bar})}. \tag{4}$$

Here we consider all the agents to be of the same mass m, so without loss of generality we set $m = 1$. Upon reaching their destination, agents are assigned with new random destinations as practiced in [13] to display a continuous motion of the agents resembling the movement in a closed environment, e.g., a mall, office, etc. Agents are also not allowed to exceed the speed limit $v_{\max} = 2$.

With these assumptions, we simulate the mobility of the agents in different environments and scenarios according to Eqs. (1)–(4) using the Euler method [23] with time steps equal to $\Delta t = 0.1$ s. These numerical simulations are similar to the methods commonly used in molecular dynamics. The robustness of the simulation with respect to the algorithm and Δt size has been validated in Appendix A 4. Agents are initially positioned randomly and uniformly across the environment. To ensure realistic initial distancing between the agents, the spreading dynamics begins four time-units after the mobility dynamics start.

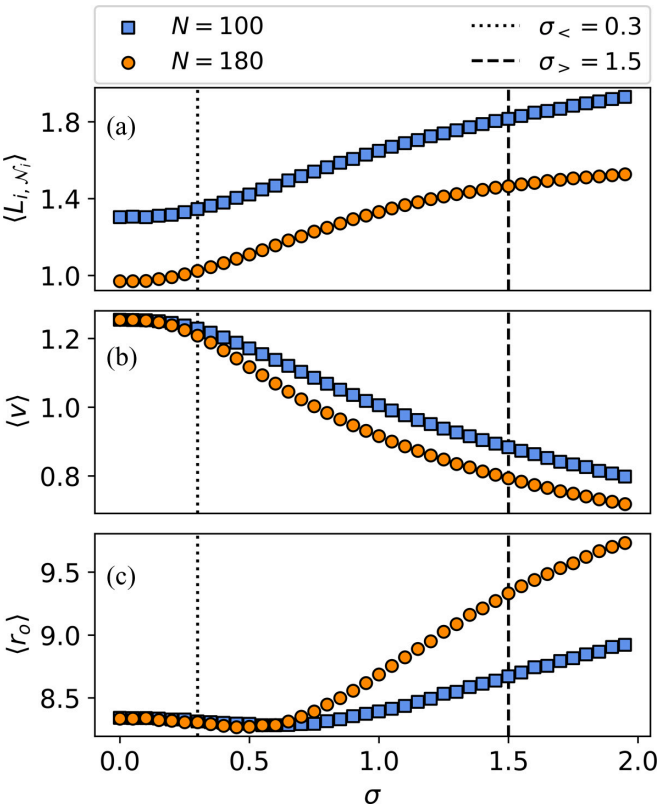

FIG. 2. Mobility quantities of agents as a function of social distancing intensity σ. The results for two different cases of $N = 100$ (blue squares) and $N = 180$ (orange circles) are presented. (a) The ensemble average of mean neighbor distance $\langle L_{i,\mathcal{N}_i}\rangle$ as a distance-based indicator between the agents. (b) The ensemble average of the agents' speeds $\langle v\rangle$ [subject to Eq. (4)]. (c) The ensemble average distance $\langle r_o\rangle$ from the origin for different values of social distancing intensity. The results show an initial slight decrease and a later increase in $\langle r_o\rangle$ explained in Fig. 4. The dotted and dashed lines, respectively, correspond to the *baseline* values of $\sigma_<$ and $\sigma_>$. Please note the discrepancy in the range of values for the three panels. *Error bars are smaller than the marker size.*

Social distancing

To go further with Eq. (2), first we set all the $\sigma_i = \sigma$ for all i. This parameter quantifies social distancing. As we intuitively expect, higher values of σ exhibit both faster reaction to nearby agents (stronger force) and larger perceived personal space (higher range).

To validate this intuition, we proceed by defining $\langle L_{i,\mathcal{N}_i}\rangle$ as the ensemble average of the mean of minimum distance between agents while $L_{i,j}$ is the pairwise distances of all agents i and j, and we define $\mathcal{N}_i = \arg\min_j(L_{i,j})$ as agent i's nearest neighbor, and $L_{i,\mathcal{N}_i}$ as agent i's minimum distance with any other agent. $\langle L_{i,\mathcal{N}_i}\rangle$ is depicted as an increasing function of σ in Fig. 2(a), therefore this average provides us with an intuition about σ since it is a good observable quantity.

B. Spreading model

To model the spreading dynamics, we use a compartmental model, categorizing the population into three compartments: S (Susceptible), E (Exposed), and I (Infectious). Agents in state S will become E upon getting into contact with the infection.

The time duration agents spend in a crowded environment is relatively shorter than the latent period for most infectious diseases [24]; therefore, E agents are not expected to become I and infect others. I agents are also not expected to recover and move to a fourth compartment R (Recovered or Removed).

Infections can occur in one of the following ways:

(i) *Direct Transmission (Person-to-Person Infection)*: Infectious agents (I) infect susceptible agents (S) in their vicinity with radius r_s, turning them to exposed E agents by the probability α_p at each time step as depicted in Fig. 1(b).

(ii) *Indirect Transmission (Environmental Infection)*: Although the mobility model is formulated in a continuous manner, in order to account for the environmental pollution, the environment is discretized into a lattice of size $L \times L$. Agents in state I contaminate the tile on which they are standing, with probability $\alpha_{p\to e}$ at each time step; on the other hand, S agents stepping on contaminated tiles get infected and turn E, with probability $\alpha_{e\to p}$ as depicted in Fig. 1(b). For simplicity, we consider $\alpha_{p\to e} = \alpha_{e\to p} = \alpha_e$. Since the duration of the simulations conducted in this study (10 min) is assumed to be much shorter than the lifetime of the virus, we can neglect the decay of the virus in the environment, i.e., the contaminated environment stays contaminated throughout the simulation. This is also in agreement with findings on the lifetime of COVID-19, which is more than a day on average [25].

While in most circumstances $\alpha_p \neq \alpha_e$, the frequency of checking the possibility of infection via both methods using a rejection-based algorithm [26] should be the same for the model to be consistent.

In this study, for the sake of simplicity and to achieve more generic results, the number of initial agents in state I will always be set equal to 1 and the rest of the agents $(N-1)$ will be initially in state S. The environment is considered to be fully sanitized prior to the simulations.

A summary of model parameters is presented in Table I, and we will explain how we fix some parameters in the next section.

TABLE I. Model parameters and constants.

N	Total number of agents
σ	Social distancing intensity (m^{-1})
$L = 30$	Environment size (m)
$\sigma_w = 5$	Barrier avoidance constant (m^{-1})
$v_i^0 = 1.3$	Agents' preferred speed (m/s)
$v_{\max} = 2$	Agents' maximum speed (m/s)
$\kappa = 7$	Social force constant (kg m^2 s^{-2})
$\kappa_w = 1$	Barrier avoidance force constant (kg m^2 s^{-2})
$r_c = 3$	Social force cutoff (m)
$r_s = 1$	Direct infection maximum distance (m)
$\tau = 0.5$	Agents' reaction time (s^{-1})
α_p	Direct infection probability
α_e	Indirect infection probability

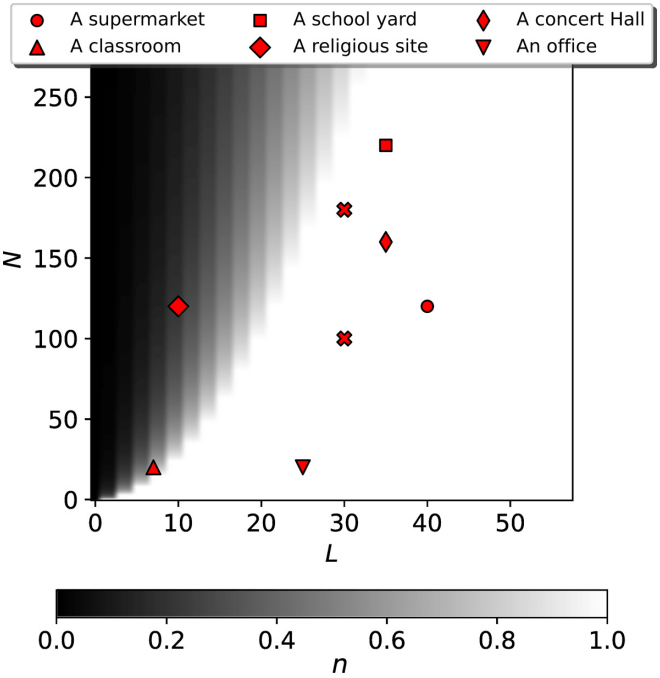

FIG. 3. The proportion of the population able to maintain a 1 m distance from each other in environments with different sizes (L^2). The markers correspond to empirical data from real-world sites: a shopping mall, a post office, the Vahdat concert hall in Tehran, Shahid Beheshti high school in Zanjan (Iran), and the Grand Mosalla mosque of Tehran (Iran) at peak hours. These data points have been normalized by different factors to only resemble the population density, not the actual size and populations. Further discussion about these data is presented in Appendix A 5. The two crosses represent the chosen data points for our simulations ($L = 30; N = 100, 180$).

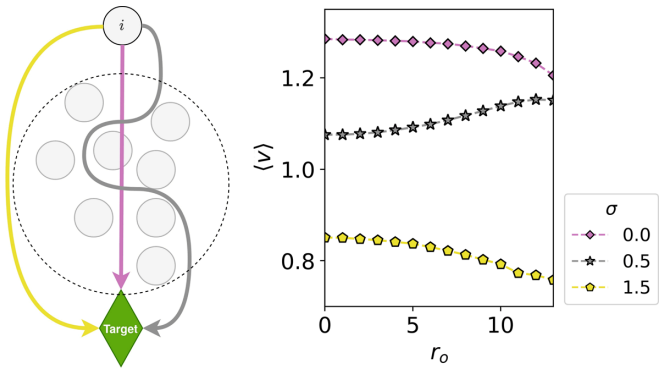

FIG. 4. The effect of swarm on agents' speed for $N = 180$. Color code indicates σ values. Left panel: A schematic illustration of the mobility of a single agent i, facing an area of high density (swarm) clustered in the center of the environment (dashed circle). With $\sigma = 0$, agent i moves directly toward its target without interacting with the other agents. With $\sigma = 1.5$ the agent moves around the swarm, increasing $\langle r_o \rangle$ of the system compared to $\sigma = 0$. With $\sigma = 0.5$ the agent moves through the swarm while making several "brakes" and minor detours from the direct path of free movement, resulting in lower speed in the central high density area. This qualitative description can be supported by the ensemble average depicted in the right panel. Right panel: The ensemble average speed for agents with r_o distance from the origin. The r_o values have been rounded to integers. For $\sigma = 0$ and $\sigma = 1.5$, $\langle v \rangle|_{r_o \to 0} > \langle v \rangle|_{r_o \gg 0}$ while for $\sigma = 0.5$, $\langle v \rangle|_{r_o \to 0} < \langle v \rangle|_{r_o \gg 0}$ *Error bars are smaller than the marker size.*

III. RESULTS

We study each parameter and its effect on the *exposure risk factor* E defined as the fraction of agents exposed to the infection. We choose parameters in ways that reflect real-world scenarios.

A. Population density

Population density is a significant factor determining the possibility of abiding by social distancing measures. To quantify this factor, we define the social distancing limit n as the proportion of the total population that are able to maintain a fixed distance from each other in a room. We can calculate n by considering an area of l^2 (l being the desired physical distancing) for each agent. $n = 1$ indicates a room in which total social distancing is *executable*, whereas $n < 1$ implies otherwise. Figure 3 demonstrates the curve separating two regimes $n < 1$ and $n = 1$. Some real-world locations are also depicted in our parameter space, based on their size and population.

For our simulation, we assume $l = r_s = 1$ m, which corresponds to the high-risk distance for COVID-19 and some other similar diseases [27]. We set $L = 30$ and choose two different scenarios for the population density where the room is filled at 0.44 and 0.8 of its maximum capacity. This would enable us to study the *effectiveness* of social distancing in the region where it is *executable* ($n = 1$). These two cases, respectively, refer to $N = 100$ and 180 and would resemble a mildly crowded and a heavily crowded environment.

B. Social distancing intensity

As discussed earlier in Sec. II A 1, we use the parameter σ to control the intensity of social distancing. To get a better real-life intuition of the parameter σ, we measure the average distance that agents keep from their nearest agent while moving in the environment in this model. The results for both population densities are provided in Fig. 2. As mentioned, the ensemble average of the agents' neighboring distances $\langle L_{i,\mathcal{N}_i} \rangle$ monotonically increases as a function of σ [Fig. 2(a)]. This increase is, however, not without a cost. To stay farther apart from other agents, each agent would have to lower their average speed and "brake" more often, resulting in a lower average speed [Fig. 2(b)] and subsequently lower efficiency of the agents in reaching their targets. Therefore, the tradeoff between social distancing and efficiency should be taken into account to set an intensity for social distancing. Near $\sigma = 0.3$ we observe that the value of $\langle v \rangle$ for the two environments begins to diverge. Based on these results, we use $\sigma_< = 0.3$ for the social force among agents in regular walking (no social distancing), as in [11], and we set $\sigma_> = 1.5$ for the case of social distancing applied by agents as an example case, in which a distance greater than r_s is maintained between the agents while leaving enough room for them to move around the environment ($\langle v \rangle > 0.7$). These choices are made without

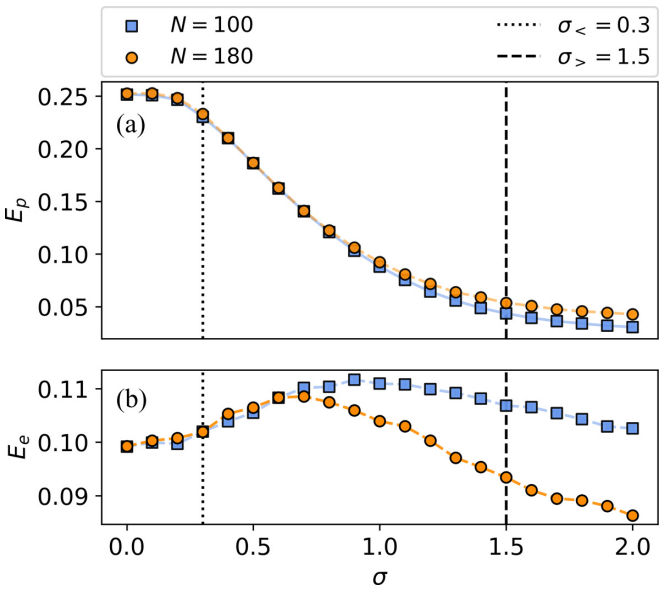

FIG. 5. The average E for different values of social distancing intensity. (a) E_p, the exposure due to direct infection. (b) E_e, the exposure due to environmental infection. The results for two different cases of $N = 100$ (blue squares) and $N = 180$ (orange circles) are presented. The dotted and dashed lines, respectively, correspond to the *baseline* values of $\sigma_<$ and $\sigma_>$. Please note the discrepancy in the range of values for the two panels. *Error bars are smaller than the marker size.*

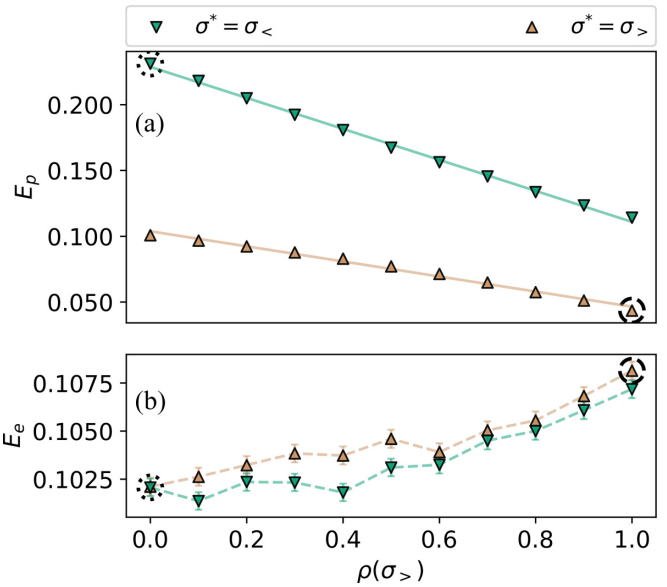

FIG. 6. The average E as a function of $\rho(\sigma_>)$, the proportion of the agents abiding by social distancing in an environment with $N = 100$. (a) E_p, the exposure due to direct infection. (b) E_e, the exposure due to environmental infection. The results for two different cases in which the initial infectious agent obeys social distancing ($\sigma^* = \sigma_>$, in khaki) and does not obey it ($\sigma^* = \sigma_<$, in dark green) are presented. The dotted and dashed circles, respectively, correspond to the *baseline* values of $\sigma_<$ and $\sigma_>$. These values signify the scenarios in which all of the population ignores ($\sigma = \sigma_<$) and abides by ($\sigma = \sigma_>$) social distancing. Please note the discrepancy in the range of values for the two panels. *Error bars in (a) are smaller than the marker size.*

the loss of generality and in order to set parameters closer to real-life situations.

In Fig. 2(c), we study $\langle r_o \rangle$, the ensemble average distance from the origin, as an indicator of the concentration of the agents. For $\sigma \to 0$, increasing σ results in a higher condensation of agents, i.e., a lower average distance from the origin, while for higher values of σ we observe the opposite effect. This counterintuitive behavior can be explained considering three different scenarios of an agent interacting with a highly dense area (swarm), as illustrated in the left panel of Fig. 4. In the $\sigma = 0$ scenario, the agent moves through the swarm without losing speed, while in the $\sigma = 1.5$ case it moves around the swarm resulting in a higher $\langle r_o \rangle$ of the system compared to $\sigma = 0$, and in the case of $\sigma = 0.5$ the agent moves through the swarm, albeit at a lower speed. This behavior results in spending more time in dense areas and effectively decreases $\langle r_o \rangle$. This analysis can be supported by Fig. 4, right panel. For $\sigma = 0$ and 1.5, the average speed of agents located at a distance r_o from the origin is a decreasing function of r_o. This decrease is due to the fact that the center of the environment ($r_o \to 0$) acts as a corridor for reaching their targets, and agents often move through this area with a higher speed. In comparison, agents move slower when they are farther away from the center of the environment, as they brake and redirect their velocity more often. For $\sigma = 0.5$ the opposite is true, and agents have relatively lower speed in the center of the environment, resulting in a lower $\langle r_o \rangle$ in comparison to $\sigma = 0$ and subsequently the initial decrease in Fig. 2(c).

We run the pedestrian and the spreading dynamics for both population regimes discussed in Sec. III A. For simplicity, we choose $\alpha_e = 2 \times 10^{-3}$ and $\alpha_p = 10^{-2}$, and later on in Sec. III D we analyze the behavior of the model for different spreading parameters. In this section we set σ uniform across all agents ($\sigma_i = \sigma$). The fraction of the exposed population over time is presented in Fig. 9 in Appendix A 1.

The average proportion of the exposed population is calculated after 10 min (600 SI time-units) of simulation time and plotted against the values of σ in Fig. 5. The first observation based on this result is that for this set of parameters, the total risk, $E = E_p + E_e$, gets reduced by the increase in social distancing. For example, for $\sigma_<$ and $\sigma_>$, the value of this reduction is $E(\sigma_<) - E(\sigma_>) = 0.207$ for $N = 180$ and $E(\sigma_<) - E(\sigma_>) = 0.181$ for $N = 100$ (the effect of social distancing in other infection parameter sets will be presented in Fig. 7). We can observe that the increase in the strength of this parameter monotonically reduces the risk of getting infected through direct infection [Fig. 5(a)].

TABLE II. Baseline parameter values.

Sign	Schematic	σ	α_p	α_e	t
dotted	· · ·	$\sigma_< = 0.3$	10^{-2}	2×10^{-3}	6×10^3 s
dashed	—	$\sigma_> = 1.5$	10^{-2}	2×10^{-3}	6×10^3 s
dash-dotted	— · —	N.A.	10^{-2}	2×10^{-3}	6×10^3 s

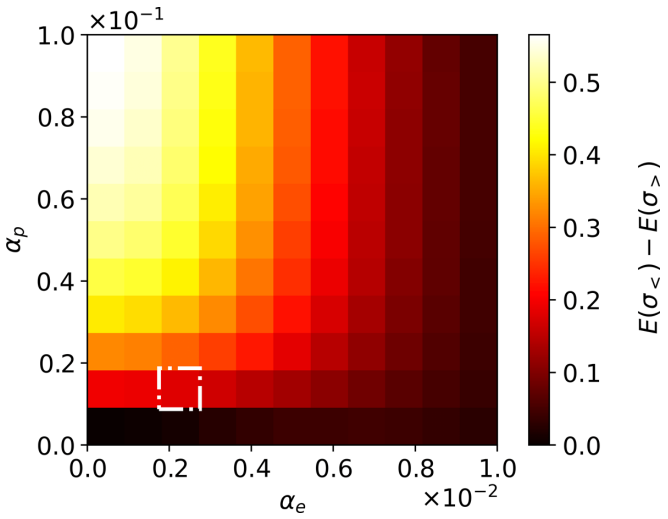

FIG. 7. The difference in the exposure risks of the two scenarios for social distancing intensity, varying α_p and α_e values. The color code indicates $E(\sigma_<) - E(\sigma_>)$. The dash-dotted pixel corresponds to the *baseline* values of $\alpha_e = 2 \times 10^{-3}$ and $\alpha_p = 10^{-2}$. Please note the discrepancy in the order of magnitude of the axes. Also note that the case in which $\alpha_e = 0$ corresponds to the case in which there is no environmental infection.

We can also see that the fraction of agents infected via environmental contamination slightly increases for both population regimes as we increase σ, but it decreases monotonically afterwards and more intensively for $N = 180$ [Fig. 5(b)]. This is partly due to the *competition* between the two methods of infection. The probability of an S agent getting indirectly infected increases when the number of susceptible agents is higher (as a result of the weakness of the direct infection). Another reason for this increase and later decrease in the value of E_e is the similar variations in the concentration of agents as a function of σ [Fig. 2(c)]. The higher concentration of agents in the central area of the environment causes higher indirect transmission. The central tiles, traversed more often by S agents, will be more likely to be contaminated as they are more often walked upon by the I agent.

C. Social distancing commonness

In this section, we study the effect of the fraction of people who abide by social distancing on the total risk factor. For this goal we divide the population into two groups, a nonabiding group with $\sigma = \sigma_< = 0.3$ and a social distancing group with $\sigma = \sigma_> = 1.5$, and we run the simulation for different proportions of people in each group. The parameter $\rho(\sigma_>)$ would represent the proportion of the agents who abide by social distancing. We analyze this matter in two different scenarios, in which the initial infectious agent is always in the former ($\sigma^* = \sigma_<$) or the latter ($\sigma^* = \sigma_>$) group. The results are presented in Fig. 6, which shows the strong effect of the behavior of the initial infectious agent on the risk factor E. In both cases, the risk of direct infection, depicted in panel (a), drops linearly as the percentage of people who abide by social distancing increases but the slope and the intercept of this linear behavior differ based on the social distancing intensity of the initial infectious agent. In other words, the risk drops by a significant factor if only the infectious agent abides by social distancing. The risk of exposure due to indirect infection, depicted in panel (b), increases as more people abide by social distancing, similar to the situation explained in Sec. III B.

TABLE III. Real-world locations data.

Shopping mall	[33]
Vahdat concert hall	Measured by the authors
High school	Measured by the authors
Grand Mosalla mosque	Measured by the authors
Post office	Measured by the authors

D. Infection parameters

To see the behavior of the dynamics in other regimes of the parameter space and in order to get a more general perspective of the model, we implement the simulations for various values of infection probabilities α_p and α_e.

In Fig. 7, we compare the overall exposure risks for $\sigma_<$ and $\sigma_>$ scenarios. As shown in this figure, there is a significant discrepancy for a wide range of infection probabilities, confirming our previous results on the effectiveness of social distancing. Due to the increasing role of direct infection and this type of infection's sensitivity to social distancing, the discrepancy increases for higher α_p and lower α_e (upper left of the diagram). Please note that for high values of α_e (right) even when α_p is high (upper right), social distancing does not play a major role. This can be explained by the *competition* between the direct and indirect transmission methods. In other words, for these values, even if the agents lower the chance of direct transmission by following the social distancing guidelines, most of them will nevertheless be exposed to the infection by the indirect transmission method.

Furthermore, to investigate the role of direct and indirect transmission, we calculate $E_p - E_e$ (Fig. 8). We observe two regimes, E_p and E_e dominated areas, respectively, denoted by red and blue, and a white area illustrating the border between the regimes. By comparing the panels, we see that due to social distancing, the E_p dominated regime has drastically shrunk in favor of E_e dominance. This observation also agrees with our previous findings that the person-to-person infection significantly decreases in the social distancing scenario ($\sigma_>$), and the environmental infection's role increases due to the higher number of available susceptible agents.

IV. SUMMARY AND DISCUSSION

We have modeled the spreading of infection among mobile agents as a combination of pedestrian dynamics and the compartmental spreading model (SEI). We defined social distancing as the intensity of social force in pedestrian dynamics, and we mapped it to the average value of the minimum distance between agents and their average speed and concentration. By taking into account both direct and indirect transmission methods of infection (Fig. 1), we have

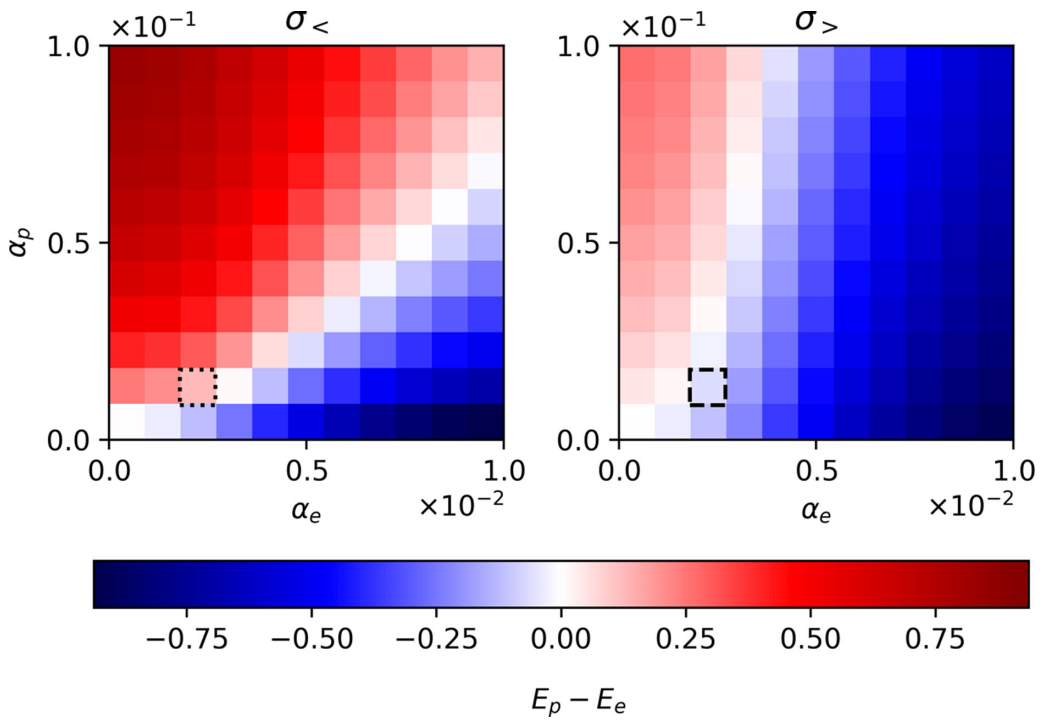

FIG. 8. The effect of social distancing on contagion regimes. $E_p - E_e$ illustrated for α_p and α_e values. Left and right panels, respectively, denote $\sigma_<$ and $\sigma_>$ scenarios for social distancing intensity. The red and blue areas, respectively, demonstrate E_p and E_e dominated areas. The dotted and dashed pixels correspond to the *baseline* values of $\alpha_e = 2 \times 10^{-3}$ and $\alpha_p = 10^{-2}$. Please note the discrepancy in the order of magnitude of the axes.

systematically evaluated the agents' exposure risks for a wide range of spreading and mobility parameters.

We observe that for social distancing to be *executable*, the population density of the environment should be under certain values (Fig. 3). As a side effect, by applying social distancing, the speed of mobile agents will decrease (Fig. 2). Although social distancing has a drastic effect on hindering the direct transmission, some of its effects can be canceled by the increase in the indirect transmission (Fig. 5), and the *effectiveness* of social distancing is dependent on the direct and indirect transmission probabilities (Fig. 7). We demonstrated the direct transmission and indirect transmission dominated regimes in the scenarios of social distancing abidance and nonabidance (Fig. 8). We also studied the *effectiveness* of social distancing when abided only by a fraction of the population (Fig. 6), and we found that even though the increase in abiding by social distancing reduces the risk of direct transmission, the social distancing measures when followed by the infected agents have the greatest effect.

According to our findings, social distancing does not always slow down the transmission, and it may counterintuitively enhance the transmission in specific regimes of σ for contagions with relatively high indirect transmission [consider Fig. 5(b) in the absence of direct transmission]. It is not clear whether this range of parameters conforms to real-world epidemic diseases, and it should be further investigated through experimental studies.

Our findings can help to determine a guideline for policymakers on how to decrease the exposure risk at public locations for many contagions such as SARS-CoV-2. The proposed model can be used to approximate the risk of exposure in a public environment where people exhibit pedestrian dynamics, such as metro stations, religious sites, leisure centers, educational campuses, etc. For example, the management board of a shopping mall can determine the decrease needed in population density in order to reduce the risk of exposure by a desired factor. In the first place, the population density of an environment should be in the region where social distancing is *executable*. Then the risk factor for this environment can be calculated via the proposed model for different populations. Now using these results, the corresponding population for a desired reduced risk factor can be derived. Afterwards, to propose a specific value for σ by considering the social distancing force's exposure risks and also its effect on the population performance, a desired σ can be proposed for the shopping mall, and the customers can be advised to keep a distance of $\langle L_{i,\mathcal{N}_i} \rangle$ as calculated in Fig. 2 for the corresponding value of σ. Also, in order to maintain social distancing and overcome the indirect transmission in the spread of infections that transmit through the environment, periodic cleaning, ventilation, and disinfecting of the environment can be conducted. Cleaning the environment would be most important in contagions with higher α_e (see Fig. 7).

Despite the capabilities mentioned above, this model has some limitations worth noting. The mobility model is limited to the environments in which the agents move around in a random manner and would not give a good approximation for the environments where the agents are stationary or have specific mobility patterns (e.g., in a bus or an airplane, where the agents are stationary most of the time). Also, the infection probabilities α_p an α_e are hard to specify for an infection. Since they are the probability of getting infected

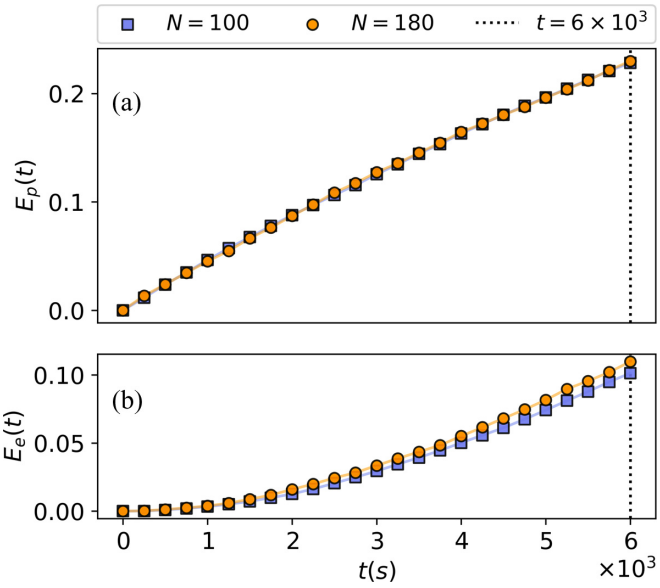

FIG. 9. The ensemble average of $E(t)$ over time for $\sigma = 0.3$. (a) $E_p(t)$ the exposure due to direct infection. (b) $E_e(t)$ the exposure due to environmental infection. The results for two different cases of $N = 100$ (blue squares) and $N = 180$ (orange circles) are presented. The dotted lines correspond to the *baseline* value of $t = 6 \times 10^3$, the duration of the simulation considered in the main part of the paper. Please note the discrepancy in the range of values for the two panels. *Error bars are smaller than the marker size.*

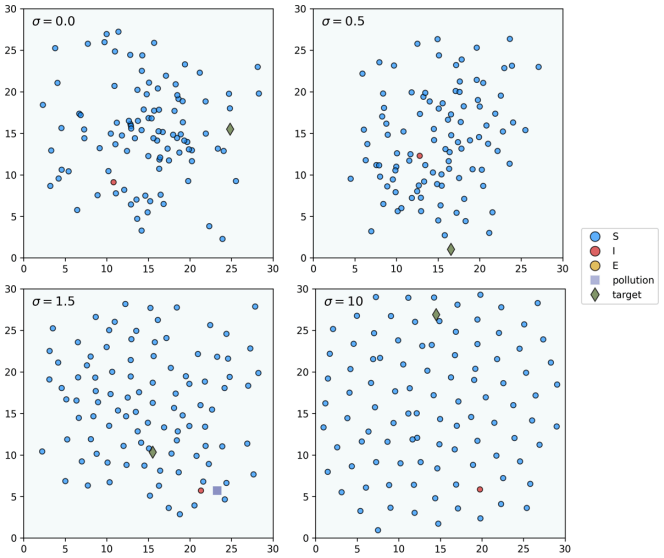

FIG. 10. The positioning of $N = 100$ agents for different σ values in a 30×30 m room. Circles represent agents, with colors indicating their status. Polluted tiles are depicted by purple squares. The green diamond indicates the target of the infectious agent at the time. Targets of other agents are not depicted for illustration purposes. While the $\langle L_{i,\mathcal{N}_i} \rangle$ is an increasing function of σ, the value of $\langle r_o \rangle$ decreases from $\sigma = 0$ to 0.5 and then increases for higher σ. An explanation of this behavior is given in Fig. 4.

in *one time step* of the simulation, they should be specified based on the simulation time step size. It should also be noted that they are not purely biological parameters. For example, talking, shaking hands, and some other social behavior can alter the value of person-to person-infection probability α_p. These social factors make the parameters harder to estimate due to the ethical and technical limitations in experiments.

For further studies, the compartmental part of the model is versatile and can be expanded to simulate long-term dynamics of the spreading by considering the E to I (exposed becoming infectious) and I to R (infectious becoming recovered) transitions. Also, this model can be combined with other empirical or random generated networks, e.g., random geometric graphs [28–30] and mean-field models. Also, in order to more realistically model the spread of airborne infections, one can alter the indirect transmission to work according to the diffusion processes to model the effect of ventilation on the spreading of the disease.

Note that apart from the environmental infection, our model is theoretically equivalent to the spreading model on the temporal spatial network of interactions between the agents where there is a connection between agents closer than r_s. It is also possible to include environmental infection by considering tiles as another type of stationary nodes, reacting differently to the infection.

The simulation and analysis is conducted by EPISTERIAN software written in Python, developed by S.S and A.H., available at [31] under GPLv3.

ACKNOWLEDGMENTS

We would like to thank M. R. Ejtehadi for his insightful comments. F.Gh. acknowledges partial support by Deutsche Forschungsgemeinschaft (DFG) under the grant project: 345463468 (idonate).

APPENDIX

1. Time evolution of the spreading

The time evolution of the exposure risk E for both direct and indirect transmission methods is depicted in Fig. 9.

2. Baseline parameter values

The dashed, dotted, and dash-dotted lines and areas illustrated in Figs. 2, 5, 6, 7, 8, and 9 correspond to the baseline values specified in Table II.

3. Illustration

Figure 10 depicts snapshots of the simulation for different values of σ. An mp4 animation demonstrating a sample realization of the dynamics can be found at [32], where circles represent agents, with colors indicating their status. Polluted tiles are depicted by purple squares. The green diamond indicates the target of the infectious agent at the time. Targets of other agents are not depicted for illustration purposes.

4. Computation robustness

Our model is composed of two parts:

(i) Mobility update (Sec. II A): at each time step of size Δt, the positions and velocities of agents are updated based on Eq. (4) via the Euler method.

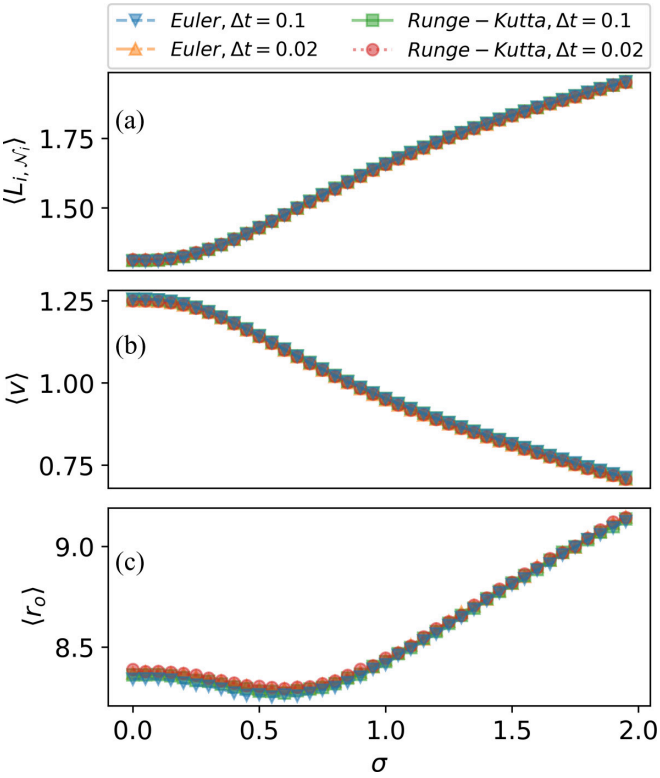

FIG. 11. Mobility quantities of agents as a function of social distancing intensity σ for different numerical methods and step-sizes. (a) The ensemble average of mean neighbor distance $\langle L_{i,\mathcal{N}_i}\rangle$ as a distance-based indicator between the agents. (b) The ensemble average of agents' speeds $\langle v\rangle$ [subject to Eq. (4)]. (c) The ensemble average distance $\langle r_o\rangle$ from the origin for different values of social distancing intensity. We observe that the mobility quantities of the dynamics are in strong agreement. Please note the discrepancy in the range of values for the three panels. *Error bars are smaller than the marker size.*

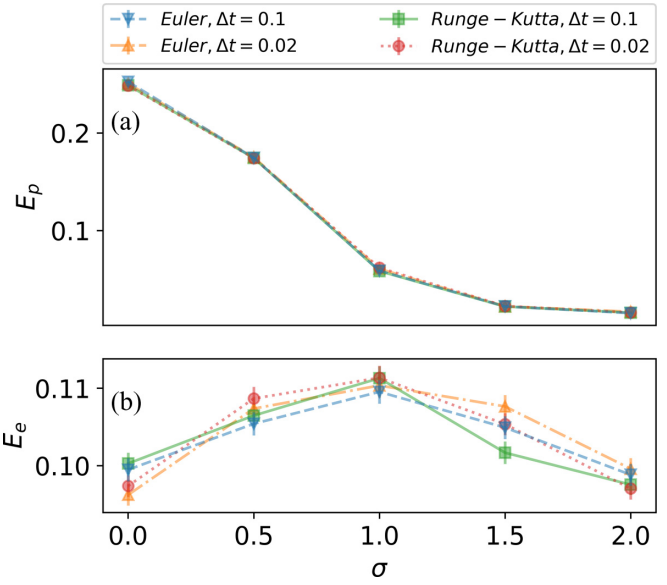

FIG. 12. The average E as a function of social distancing intensity σ for different numerical methods and step-sizes. (a) E_p, the exposure due to direct infection. (b) E_e, the exposure due to environmental infection for different numerical methods and step-sizes. The dotted and dashed lines, respectively, correspond to the *baseline* values of $\sigma_<$ and $\sigma_>$. We observe that the infection results of the dynamics are in strong agreement. Please note the discrepancy in the range of values for the two panels. *Error bars are smaller than the marker size for the top panel.*

(ii) Spreading update (Sec. II B): at each time step of size $\widetilde{\Delta t}$, S agents prone to indirect transmission (agents standing on polluted tiles) or direct transmission (closer than r_s to an infectious agent) become E by probabilities α_e and α_p, respectively. This scheme is known to be a rejection-based algorithm [26], meaning that at each step, the proposal to update the system state (here $S \to E$) is either accepted by its corresponding probability or it is rejected.

Throughout the main part of the paper, we have considered $\Delta t = \widetilde{\Delta t} = 0.1$ s.

To check the robustness of the dynamics for different algorithms and time step-sizes, we consider both the Euler and the fourth-order Runge-Kutta [23] numerical methods with time step-sizes, $\Delta t = 0.1$ and 0.02 s for the mobility dynamics of the agents. In Figs. 11 and 12, respectively, we observe the mobility and infection results of the dynamics for these methods of integration in strong agreement.

Note that we still preserve the value of $\widetilde{\Delta t}$ to be equal to 0.1 s, as altering this parameter would obviously change the exposure results, e.g., halving $\widetilde{\Delta t}$ would double the exposure opportunities in the same time interval.

5. Sources of the real-world data

The estimated population densities presented in Fig. 3 are obtained from the sources specified in Table III. The area and average resident population have been empirically estimated or calculated based on the data from sample locations in Iran. Since the actual numbers are not essential for the purpose of this study and they are just presented as arbitrary examples, we have avoided specific discussion about each one. Please note that the values are normalized in order for the densities to be comparable to each other (e.g., comparing a large mosque with a classroom).

[1] *Social Distancing, Quarantine, and Isolation* (CDC-NCIRD-DVD).

[2] W. O. Kermack, A. G. Mckendrick, and G. T. Walker, A contribution to the mathematical theory of epidemics, Proc. Royal Soc. A **115**, 700 (1927).

[3] M. J. Keeling and P. Rohani, *Modeling Infectious Diseases in Humans and Animals* (Princeton University Press, Princeton, NJ, 2011).

[4] M. E. J. Newman, *Networks an Introduction* (Oxford University Press, Oxford, 2018).

[5] A. Barrat, M. Barthelemy, and A. Vespignani, *Dynamical Processes on Complex Networks* (Cambridge University Press, Cambridge, 2008).

[6] N. Masuda and P. Holme, *Temporal Network Epidemiology* (Springer, Singapore, 2017).

[7] P. Holme and S. Jari, *Temporal Networks* (Springer-Verlag, Berlin, Heidelberg, 2013).

[8] M. Karsai, M. Kivelä, R. K. Pan, K. Kaski, J. Kertész, A. L. Barabási, and J. Saramäki, Phys. Rev. E **83**, 025102 (2011).

[9] J. P. Rodríguez, F. Ghanbarnejad, and V. M. Eguíluz, Risk of coinfection outbreaks in temporal networks: A case study of a hospital contact network, Front. Phys. **5**, 46 (2017).

[10] S. Sajjadi, M. R. Ejtehadi, and F. Ghanbarnejad, Impact of temporal correlations on high risk outbreaks of independent and cooperative SIR dynamics, PLoS ONE **16**, e0253563 (2021).

[11] D. Helbing and P. Molnar, Social force model for pedestrian dynamics, Phys. Rev. E **51**, 4282 (1995).

[12] S. Namilae, A. Srinivasan, A. Mubayi, M. Scotch, and R. Pahle, Self-propelled pedestrian dynamics model: Application to passenger movement and infection propagation in airplanes, Physica A **465**, 248 (2017).

[13] T. Harweg, D. Bachmann, and F. Weichert, Agent-based simulation of pedestrian dynamics for exposure time estimation in epidemic risk assessment, arXiv:2007.04138.

[14] S. Namilae, P. Derjany, A. Mubayi, M. Scotch, and A. Srinivasan, Multiscale model for pedestrian and infection dynamics during air travel, Phys. Rev. E **95**, 052320 (2017).

[15] D. Kim and A. Quaini, Coupling kinetic theory approaches for pedestrian dynamics and disease contagion in a confined environment, arXiv:2003.08357.

[16] L. Goscé, D. A. W. Barton, and A. Johansson, Analytical modelling of the spread of disease in confined and crowded spaces, Sci. Rep. **4**, 4856 (2015).

[17] Y. Xiao, M. Yang, Z. Zhu, H. Yang, L. Zhang, and S. Ghader, Transport Policy **109**, 12 (2021).

[18] A. Bouchnita and A. Jebrane, A multi-scale model quantifies the impact of limited movement of the population and mandatory wearing of face masks in containing the COVID-19 epidemic in Morocco, Math. Modell. Nat. Phenom. **15**, 31 (2020).

[19] P. Derjany, S. Namilae, D. Liu, and A. Srinivasan, Multiscale model for the optimal design of pedestrian queues to mitigate infectious disease spread, PLOS ONE **15**, e0235891 (2020).

[20] U. D. of Health, H. Services, *et al.*, Principles of epidemiology in public health practice third edition an introduction to applied epidemiology and biostatistics, Atlanta, GA, Available on the website: https://www.cdc.gov/csels/dsepd/ss1978/SS1978.pdf, Vol. 8 (2013).

[21] C. Castellano, S. Fortunato, and V. Loreto, Statistical physics of social dynamics, Rev. Mod. Phys. **81**, 591 (2009).

[22] R. C. Browning, E. A. Baker, J. A. Herron, and R. Kram, Effects of obesity and sex on the energetic cost and preferred speed of walking, J. Appl. Physiol. **100**, 390 (2006).

[23] K. A. Atkinson, *An Introduction to Numerical Analysis*, 2nd ed. (Wiley, New York, 1989).

[24] N. M. Linton, T. Kobayashi, Y. Yang, K. Hayashi, A. R. Akhmetzhanov, S. M. Jung, B. Yuan, R. Kinoshita, and H. Nishiura, Incubation period and other epidemiological characteristics of 2019 novel coronavirus infections with right truncation: A statistical analysis of publicly available case data, J. Clin. Med. **9**, 538 (2020).

[25] N. van Doremalen, T. Bushmaker, D. H. Morris, M. G. Holbrook, A. Gamble, B. N. Williamson, A. Tamin, J. L. Harcourt, N. J. Thornburg, S. I. Gerber, J. O. Lloyd-Smith, E. de Wit, and V. J. Munster, Aerosol and surface stability of sars-cov-2 as compared with sars-cov-1, N. Engl. J. Med. **382**, 1564 (2020).

[26] C. L. Vestergaard and M. Génois, Temporal gillespie algorithm: Fast simulation of contagion processes on time-varying networks, PLoS Comput. Biol. **11**, e1004579 (2015).

[27] World Health Organization, Coronavirus disease (covid-19) advice for the public, available online: https://www.who.int/emergencies/diseases/novel-coronavirus-2019/advice-for-public, 2020.

[28] M. Barthélemy, Spatial networks, Phys. Rep. **499**, 1 (2011).

[29] J. P. Rodríguez, F. Ghanbarnejad, and V. M. Eguíluz, Particle velocity controls phase transitions in contagion dynamics, Sci. Rep. **9**, 6463 (2019).

[30] J. Dall and M. Christensen, Random geometric graphs, Phys. Rev. E **66**, 016121 (2002).

[31] https://github.com/ialireza13/Episterian.

[32] See Supplemental Material at http://link.aps.org/supplemental/10.1103/PhysRevE.104.014313. for a sample animation of the dynamics.

[33] Walmart retail corporation made changes in their shopping process to encourage social distancing, as explained in the following article on their website: Changes to our shopping process to encourage social distancing, https://corporate.walmart.com/newsroom/2020/04/03/changes-to-our-shopping-process-to-encourage-social-distancing.